Polar Residues in the Protein Core of *Escherichia coli* Thioredoxin Are Important for Fold Specificity†

Daniel N. Bolon‡ and Stephen L. Mayo*,§

Biochemistry Option, California Institute of Technology, Mail Code 147-75, Pasadena, California 91125, and Howard Hughes Medical Institute and Division of Biology, California Institute of Technology, Mail Code 147-75, Pasadena, California 91125

Received March 1, 2001; Revised Manuscript Received June 5, 2001

ABSTRACT: Most globular proteins contain a core of hydrophobic residues that are inaccessible to solvent in the folded state. In general, polar residues in the core are thermodynamically unfavorable except when they are able to form intramolecular hydrogen bonds. Compared to hydrophobic interactions, polar interactions are more directional in character and may aid in fold specificity. In a survey of 263 globular protein structures, we found a strong positive correlation between the number of polar residues at core positions and protein size. To probe the importance of buried polar residues, we experimentally tested the effects of hydrophobic mutations at the five polar core residues in *Escherichia coli* thioredoxin. Proteins with single hydrophobic mutations (D26I, C32A, C35A, T66L, and T77V) all have cooperative unfolding transitions like the wild type (wt), as determined by chemical denaturation. Relative to wt, D26I is more stable while the other point mutants are less stable. The combined 5-fold mutant protein (IAALV) is less stable than wt and has an unfolding transition that is substantially less cooperative than that of wt. NMR spectra as well as amide deuterium exchange indicate that IAALV is likely sampling a number of low-energy structures in the folded state, suggesting that polar residues in the core are important for specifying a well-folded native structure.

The clustering of hydrophobic residues in protein cores is a general feature of globular proteins in their native state (*1*, *2*). In the denatured state, these hydrophobic residues become exposed to solvent. The interaction of hydrophobic amino acids with water compared with hydrophobic−hydrophobic interactions results in the thermodynamically unfavorable ordering of solvent atoms in the denatured state. Thus, the burial of hydrophobic surface area upon protein folding is expected to thermodynamically stabilize the native state relative to the unfolded state (*3*, *4*). Experimental evidence abounds for this stabilization. For example, an increased level of hydrophobic burial in the design of the β1 domain of protein G resulted in a molecule with dramatically improved thermostability (*5*), while cavity-forming mutations that reduced the level of hydrophobic burial were destabilizing in T4 lysozyme (*6*). Simple lattice models suggest that the clustering of solvent-averse side chains in the protein interior is sufficient to encode a unique compact chain conformation (*7*). Experimentally, the restriction of core residues to hydrophobic identity has been successfully employed in the design of a 28-residue $\beta\beta\alpha$ motif (*8*).

The transfer of polar amino acids from water to hydrophobic solvent results in a loss of hydrogen bonding and is thermodynamically unfavorable (*9*). In the unfolded state, polar residues are largely solvated and form hydrogen bonds to water (*10*, *11*). As expected, polar residues that are buried in the folded state and fail to make intramolecular hydrogen bonds are destabilizing relative to hydrophobic residues (*12*, *13*). Buried polar residues can reduce the free energy of folding by forming intramolecular hydrogen bonds. However, this decrease in free energy can be offset by gains in free energy due to desolvation (*14*) and the entropy loss associated with fixing side chains (*15*). To address this energetic balance, a number of experimental studies have measured the thermodynamic effect of replacing a side chain that forms an intramolecular hydrogen bond in the folded state with a residue that cannot form a hydrogen bond (*16*−*19*). While disagreement exists, interpretation of the experimental data indicates that an intramolecular hydrogen bond can stabilize the native state on the order of 1 kcal/mol (*20*).

Structural specificity, the capacity to form a single unique folded structure, has been well studied in coiled coil systems where experimental techniques exist for rapidly identifying a parallel or antiparallel orientation as well as an oligomeric state. Coiled coils contain a heptad repeat denoted **abcdefg** where positions **a** and **d** form the interface between the helices, positions **e** and **g** are at the interface boundary, and positions **b**, **c**, and **f** are oriented toward solvent. Kim and co-workers systematically changed residues in the GCN4 homodimeric coiled coil into the Fos-Jun heterodimeric coiled coil. It was found that eight polar residues at the **e** and **g** positions from Fos-Jun in the GCN4 background specified heterodimer formation over homodimer formation (*21*). Buried hydrogen bonds between an asparagine side chain at an **a** position from each monomer are found in the

† This research was supported by the Howard Hughes Medical Institute and the Ralph M. Parsons Foundation (S.L.M.), the Helen G. and Arthur McCallum Foundation, the Evelyn Sharp Graduate Fellowship, and Grant GM07616 from the National Institutes of Health (D.N.B.).

* To whom correspondence should be addressed. E-mail: steve@mayo.caltech.edu.

‡ Biochemistry Option.

§ Howard Hughes Medical Institute and Division of Biology.

10.1021/bi010427y CCC: $20.00
Published on Web 08/01/2001

homodimeric coiled coil domain of GCN4 (*22*). When this asparagine is replaced with valine (*23*) or aminobutyric acid (*24*), a mixture of dimers and trimers is formed. Crystal structures of the aminobutyric acid mutant demonstrate that the hydrophobic core is able to pack efficiently in both the dimeric and trimeric states (*24*). A parallel heterodimeric coiled coil dubbed "peptide velcro" was successfully designed with an asparagine from each monomer forming buried hydrogen bonds as in GCN4 as well as charged residues at the **e** and **g** positions that are complemented in the parallel structure but not in the antiparallel structure (*25*). When the buried asparagine in this coiled coil was replaced with leucine, the resulting molecule formed a heterotetramer that lacked a unique orientation of the helices (*26*). In coiled coil systems, buried polar residues clearly play a role in structural specificity.

The role of polar residues in the core of globular proteins has not been studied as extensively. We analyzed the number of polar residues at core positions in 263 globular proteins from a previously published structural data set (*27*). We find a strong positive correlation between protein size and the number of polar residues at core positions. Active site residues that are often buried in proteins are not prevalent enough to fully account for the number of polar residues observed at core positions, suggesting that core polar residues play a structural role. To evaluate this possible structural role, the effect of polar to hydrophobic mutations was experimentally determined in a model system, the 108-residue protein *Escherichia coli* thioredoxin. The ORBIT (optimization of rotamers by iterative techniques) protein design software (*8*) was used to predict hydrophobic mutations compatible with the wild-type protein structure (*28*). Thermodynamic as well as NMR[1] data indicate that core polar residues in thioredoxin aid in distinguishing a single well-folded structure from alternative structures.

EXPERIMENTAL PROCEDURES

Analysis of Polar Residues at Core Positions in Protein Structures. The orientation of the C$\alpha-C\beta$ vector relative to a solvent-accessible surface computed with only the template Cα atoms was used to determine core positions as previously described (*29*). Briefly, a position was classified as core if the distance from its Cα atom, along its C$\alpha-C\beta$ vector, to the solvent accessible surface was greater than 5.0 Å, and if the shortest distance from its Cβ atom to the surface was greater than 2.0 Å. The following 10 amino acids were considered polar: Arg, Asn, Asp, Cys, Gln, Glu, His, Lys, Ser, and Thr.

Computational Modeling. Simulations were performed using coordinates from the 1.7 Å X-ray structure of thioredoxin (*28*). The five polar core positions in wild-type (wt) thioredoxin (D26, C32, C35, T66, and T77) were restricted to the following seven amino acids: Ala, Val, Leu, Ile, Phe, Tyr, and Trp. Side chains at other core positions in the protein were allowed to change geometry while retaining their wt identity. The remainder of the structure was held fixed during the optimization. The resulting combinatorial complexity is

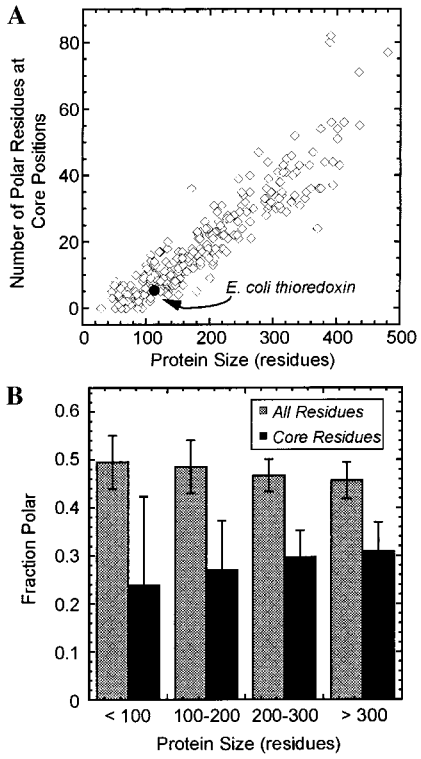

FIGURE 1: (A) Correlation of the number of polar residues at core positions with protein size. (B) Fraction of residues that are polar as a function of protein size. Error bars indicate one standard deviation from the mean.

10^{28} possible rotamer (side chain identity and geometry) sequences. Computational details and potential functions are described in our previous work (*8*). Similar calculations were also performed that optimized the identity of each polar core residue independently.

Mutagenesis and Protein Purification. The genes for all variants were constructed by inverse PCR (*30*) using the gene for wt thioredoxin (Invitrogen) cloned into pET-11a (Novagen). Mutations were confirmed by DNA sequencing. BL21(DE3) hosts (Invitrogen) were used for protein expression. Cells were grown to mid log phase and induced with 0.5 mM IPTG (ICN) for 3 h at 37 °C. Cells were lysed by sonication and centrifuged twice at 20000*g* for 30 min. Acetonitrile (EM Science) was added to the soluble fraction to a final concentration of 60%. After centrifugation, the supernatant was evaporated to half its volume and purified by reverse phase high-performance liquid chromatography using an acetonitrile/water gradient containing 0.1% trifluoroacetic acid (Applied Biosystems). Protein identities were confirmed by mass spectrometry. Protein concentrations were determined by UV absorbance in 7 M GdmCl (ICN) based on an extinction coefficient of 13 700 M^{-1} cm^{-1} at 280 nm (*31*).

CD Analysis. CD data were collected on an Aviv 62DS spectrometer equipped with a thermoelectric unit and using a 1 cm path length cell. Protein samples were 5 μM in 50 mM sodium phosphate (pH 7.0). Guanidinium chloride denaturations were monitored at 219 nm and 25 °C for comparison to previously published data (*32*). ΔG values, *m* values, and error estimates were obtained by fitting the denaturation data to a two-state transition as described previously (*33*). The GdmCl concentration was measured by refractometry.

[1] Abbreviations: CD, circular dichroism; DSC, differential scanning calorimetry; NMR, nuclear magnetic resonance; T_m, melting temperature; ΔG, free energy of unfolding; *m* value, slope of ΔG versus denaturant concentration; C_m, midpoint of the guanidinium chloride unfolding transition; GdmCl, guanidinium chloride.

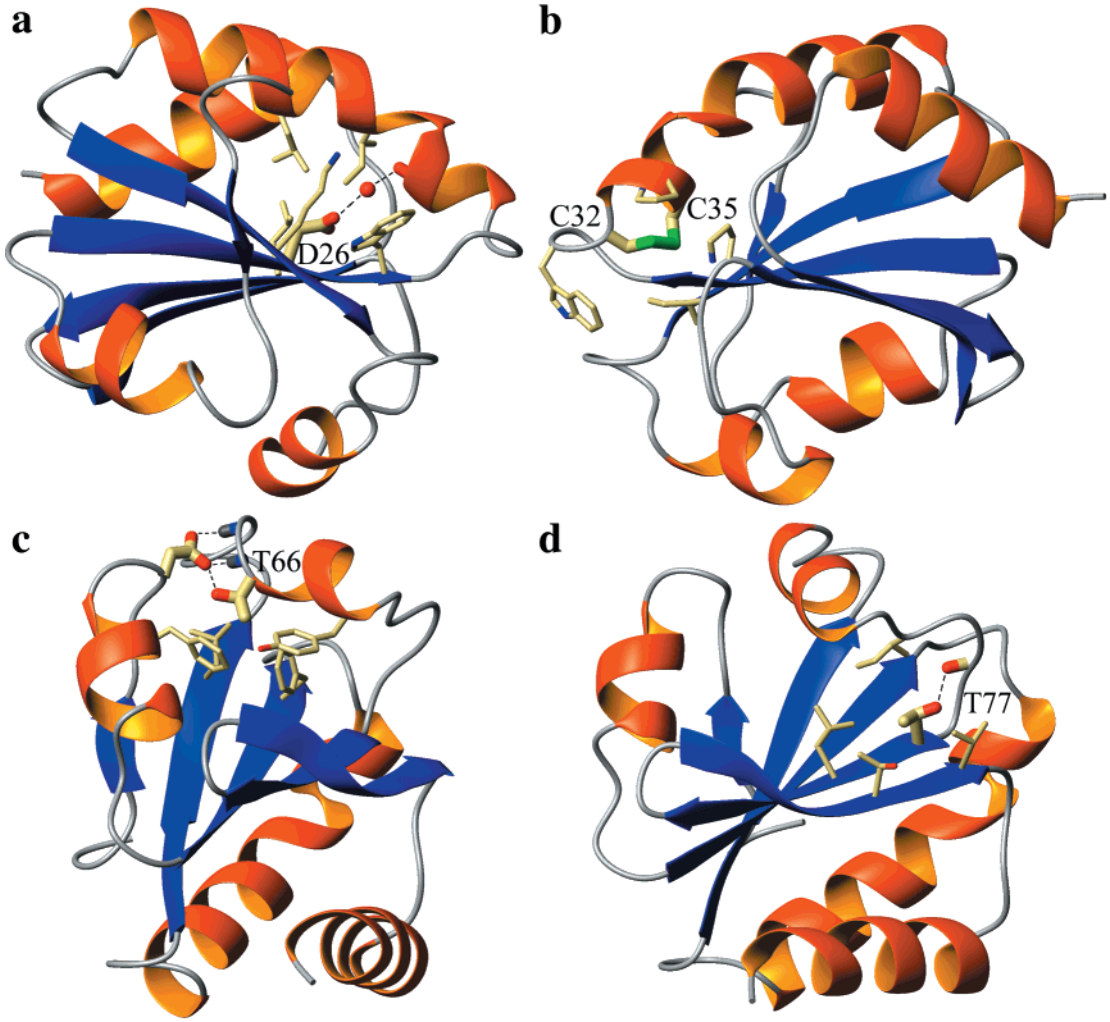

FIGURE 2: Ribbon diagrams of the X-ray crystal structure of wild-type *E. coli* thioredoxin (*28*) illustrating polar residues in the core and their surrounding contacts. (A) Asp26 makes a putative water-mediated hydrogen bond with the carbonyl oxygen of Cys35. (B) Cys32 and Cys35 form an intramolecular disulfide bond. (C) Thr66 makes a hydrogen bond to the side chain of Asp9. (D) Thr77 hydrogen bonds to the carbonyl oxygen of Gly74. These structures were generated using MOLMOL (*47*).

Fluorescence Analysis. Fluorescence measurements were taken on an SLM 8000 spectrofluorimeter. Chemical denaturation of the wild type and IAALV (D26I/C32A/C35A/T66L/T77V) were determined by fluorescence. Protein samples were at 5 μM in 50 mM sodium phosphate (pH 7.0). Samples were excited at 280 nm, and chemical denaturation was followed by emission at a wavelength of 340 nm.

DSC. Protein samples at ~0.7 mg/mL were dialyzed against 50 mM sodium phosphate buffer (pH 7.0). DSC data were collected on an N-DSC II instrument from Calorimetric Sciences Corp. (*34*). Samples were degassed under vacuum for 15 min prior to scanning. Scans were performed at a rate of 1.0 °C/min. Data were analyzed using the program cpcalc (Applied Thermodynamics).

NMR Spectroscopy. Protein samples at 0.5 mM were prepared in a 90:10 H_2O/D_2O mixture buffered at pH* 7.0 with 50 mM sodium phosphate. Spectra were acquired on a Varian Inova 600 MHz spectrometer at 25 °C. For hydrogen exchange studies, an NMR sample was prepared, the pH was adjusted to 7.0, and a spectrum was acquired to serve as an unexchanged reference. This sample was lyophilized and reconstituted in 99.9% D_2O, and repetitive acquisition of spectra was begun immediately at a rate of one spectrum per 100 s. Data acquisition continued for ~20 h, and then the sample was heated above its calorimetrically determined melting temperature for 15 min to fully exchange all labile protons. After the sample was cooled to 25 °C, a final spectrum was acquired to serve as the fully exchanged reference. The areas of all exchangeable amide peaks were normalized to that of a nonexchanging aliphatic proton peak.

RESULTS

We find a strong positive correlation between the number of polar residues at core positions and protein size (Figure 1A). The largest protein in our analysis with no polar core residues was 94 amino acids. The number of polar residues at core positions as a function of the number of core residues was also analyzed (data not shown). According to a linear fit, a protein with eight or more core residues is expected to have at least one polar residue at a core position, and for proteins with a large number of core residues, approximately one-third of the core residues are polar. The largest number of core residues in a protein with no core polar residues was 27. The average fraction of residues in the core that are polar increases slightly as protein size increases in the following ranges: fewer than 100, 100−200, 200−300, and more than 300 residues (Figure 1B). The average within each size range is within a standard deviation of the other size ranges.

Table 1: Experimental Thermodynamic Data

protein	T_m[a] (°C)	ΔG[b] (kcal mol^{-1})	C_m[c] (M)	m value[d] (kcal mol^{-1} M^{-1})
wt	87	9.0	2.6	3.4
reduced wt	76	6.3	1.8	3.6
D26I	98	12.1	3.7	3.3
C32A	74	5.3	1.6	3.4
C35A	73	5.9	1.7	3.5
T66L	85	7.6	2.4	3.1
T77V	82	7.9	2.5	3.2
AALV	55	2.8	1.0	2.8
IAALV	66	3.9	2.4	1.6

[a] Calorimetrically determined melting temperature. [b] Free energy of unfolding at 25 °C measured by guanidinium chloride denaturation (monitored by CD). [c] Midpoint of the guanidinium chloride unfolding transition. [d] Slope of ΔG vs denaturant concentration plots.

Similarly, previous research has shown that larger proteins tend to bury a larger percentage of the accessible surface area of their polar uncharged and charged atoms (*35*). The average fraction of all residues that are polar decreases slightly with increased protein size within the same ranges, and the average from each size range is again within a standard deviation of the other size ranges.

Side chains of the five polar core residues (D26, C32, C35, T66, and T77) in *E. coli* thioredoxin are greater than 95% buried, are distant in space from each other with the exception of the disulfide-bonded cystine, and make a range of hydrogen bonding interactions in the 1.7 Å crystal structure (*28*). D26, C32, C35, and T77 are conserved in human thioredoxin, which has a 0.79 Å rmsd from the *E. coli* structure and whose sequence is 29% identical with *E. coli* thioredoxin (*36*). The protein atoms surrounding D26 in *E. coli* thioredoxin are hydrophobic (Figure 2A). One of the Oδ atoms of D26 is solvent inaccessible, while the other is slightly solvent accessible via a narrow cleft in the protein. There is a water molecule in this cleft within hydrogen bonding distance (2.7 Å) of D26. This water is also within hydrogen bonding distance of the carbonyl oxygen of C35 (2.8 Å). A water molecule making similar contacts is present in both of the crystallographically independent molecules of the 1.7 Å structure (*28*) and the structure of a point mutant of *E. coli* thioredoxin (*37*), and is found in five of six structures of human thioredoxin (*36*, *38*). C32 and C35 form a redox active disulfide bond in wt thioredoxin. They are located close to the boundary between the protein core and surface. C32 and C35 are both slightly solvent exposed (Figure 2B); however, the sulfur atoms are solvent inaccessible. The sulfur atom of C32 is within weak hydrogen bonding distance of the amide nitrogen of C35 (3.2 Å). T66 is solvent inaccessible (Figure 2C) and is within hydrogen bonding distance of the side chain of D9 which makes putative hydrogen bonds with the amide protons of both T66 (3.0 Å) and G65 (2.9 Å). T77 is slightly solvent accessible (Figure 2D) and makes a putative hydrogen bond with the carbonyl oxygen of G74 (2.7 Å).

The ORBIT protein design calculations recommended the following five polar to hydrophobic mutations in thioredoxin: D26I, C32A, C35A, T66L, and T77V. Identical mutations were predicted when each position was optimized individually. Four of the point mutant proteins (C32A, C35A, T66L, and T77V) were thermodynamically destabilized relative to wt, while D26I was stabilized (Table 1). AALV, a mutant protein combining the four destabilizing mutations

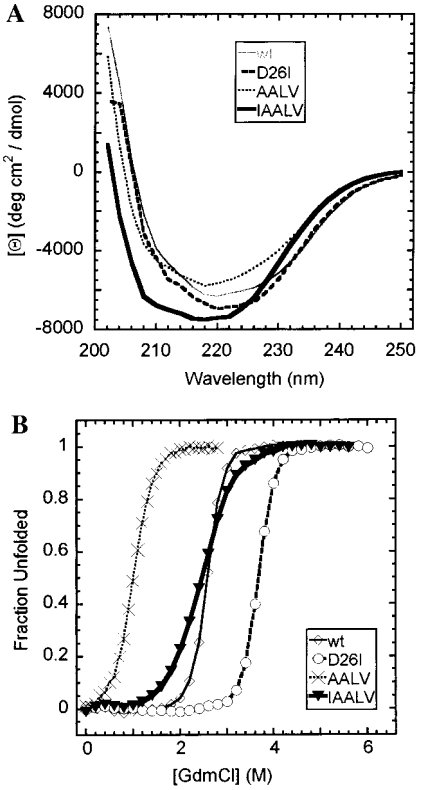

FIGURE 3: Circular dichroism measurements of wt, D26I, AALV (C32A/C35A/T66L/T77V), and IAALV (D26I/C32A/C35A/T66L/T77V) thioredoxin. (A) Far-UV CD spectra. (B) Guanidinium chloride denaturation at 25 °C monitored by CD at 219 nm.

(C32A/C35A/T66L/T77V), was thermodynamically destabilized relative to wt, but had a CD spectrum similar to that of wt (Figure 3A) and an unfolding transition with cooperativity similar to that of wt as observed by chemical denaturation monitored by CD (Figure 3B). The 5-fold mutant protein IAALV (D26I/C32A/C35A/T66L/T77V) is less stable than wt and has an unfolding transition that is substantially less cooperative than those of D26I, AALV, and wt as observed by chemical denaturation monitored by CD (Figure 3B). When the transitions are monitored by fluorescence, chemical unfolding experiments also exhibit a substantially less cooperative unfolding transition for IAALV than for wt (m values of 2.1 and 3.3 kcal mol^{-1} M^{-1}, respectively). Comparison of the extent of chemical denaturation as monitored by CD and fluorescence does not indicate the presence of intermediate states.

The thermodynamic stability of D26I is 3.1 kcal/mol greater than that of the wild type. Hydrogen exchange (Figures 4 and 5) shows that D26I protects slightly more amide protons than wild-type thioredoxin. The thermodynamic stability of IAALV is 1.1 kcal/mol greater than that of AALV. IAALV has very few protected amide protons relative to AALV; however, these protons are well protected (Figures 4 and 5). The proton NMR spectrum (Figures 4 and 6) of D26I shows slight line broadening relative to wild-type thioredoxin. IAALV shows considerable line broadening and loss of chemical shift dispersion relative to AALV (Figures 4 and 6).

DISCUSSION

The increased thermodynamic stability of D26I relative to the wild type at neutral pH is similar to that reported for

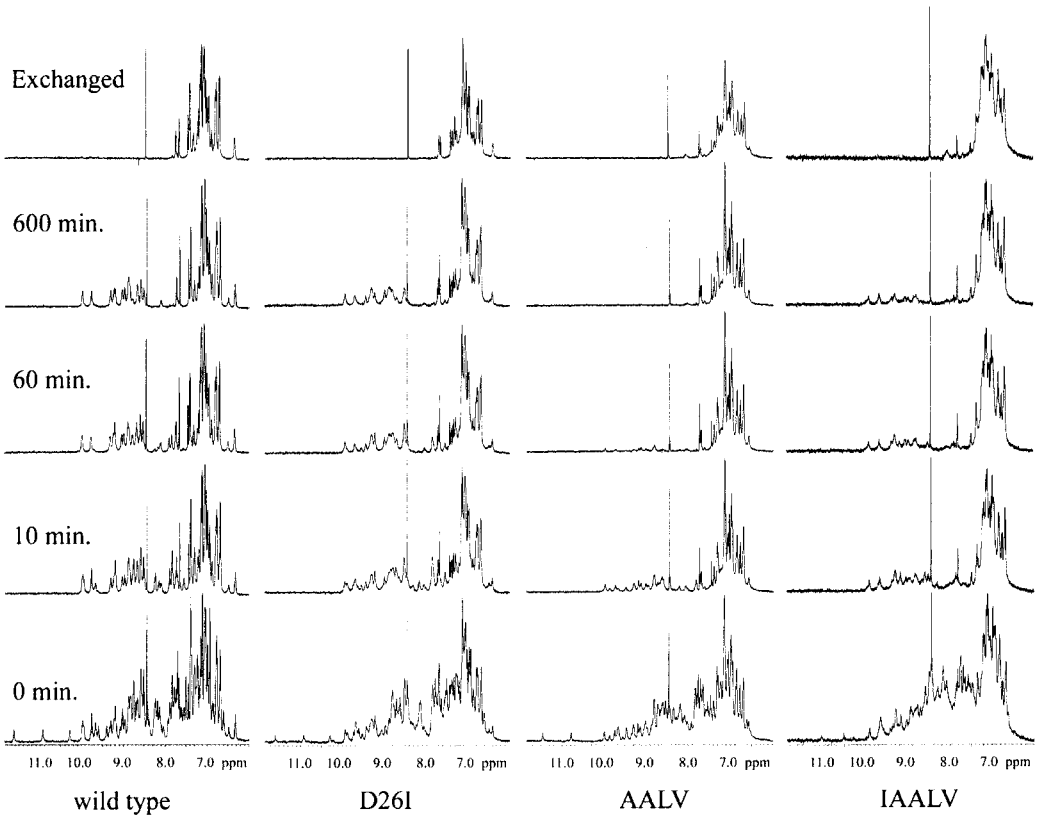

FIGURE 4: Proton NMR spectra of wt, D26I, AALV (C32A/C35A/T66L/T77V), and IAALV (D26I/C32A/C35A/T66L/T77V) thioredoxin. The spectra at 0 min were recorded in a 90:10 H_2O/D_2O mixture, and additional times refer to exchange time after resuspension of the lyophilized sample in 99.9% D_2O. The fully exchanged spectra were acquired after heating the samples above their calorimetrically determined melting temperature. IAALV has broader lines and poorer dispersion than wt, suggesting that IAALV exhibits greater conformational flexibility. The persistence of amide peaks at 600 min is an indication of well-protected protons in IAALV. Spectra at 0 min were scaled to maximize the height of the viewable area. Within columns, spectra are scaled identically. The sharp peaks at 8.45 ppm are impurities.

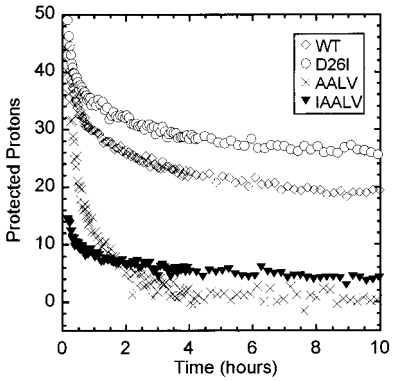

FIGURE 5: Amide hydrogen−deuterium exchange of wt, D26I, AALV (C32A/C35A/T66L/T77V), and IAALV (D26I/C32A/C35A/T66L/T77V) thioredoxin. Total area of exchangeable peaks, expressed as the number of protons, as a function of time at 25 °C and pH 7.0. Exchange rates calculated with the program SPHERE (*48*, *49*) using the wt thioredoxin sequence predict a protection factor of 10^4 corresponds to an average half-life of 0.97 h under these conditions.

D26A (*39*). The midpoint of guanidinium chloride denaturation increases by 1.1 M for D26I and 0.9 M for D26A (*39*) relative to that of the wild type. In both cases, the increased thermodynamic stability relative to that of wt is likely due to the removal from the core of a charged atom whose hydrogen bond potential was unsatisfied (*39*). The protected protons as well as the chemical denaturation data suggest that D26I is well folded. However, the line shape in the NMR spectrum of D26I is poorer than that for wt, indicating some structural differences. The thermodynamic destabilization of T66L and T77V relative to wt is likely due to the loss of intramolecular hydrogen bonds without compensatory interactions with solvent for the previous hydrogen bond partners (Oδ of Asp9 and O of Gly74).

The loss in stability of the cysteine to alanine variants (C32A and C35A) relative to wt can largely be ascribed to removal of the disulfide cross-link. Calorimetric studies by Sturtevant and co-workers (*40*) compared reduced wild-type and C32S/C35S thioredoxin and found an increased enthalpy of unfolding for C32S/C35S relative to the reduced wild-type protein. From this study, it was concluded that stronger hydrogen bonding by the more polarizable hydroxyl of serine relative to the sulfhydryl of cysteine explained the difference in calorimetric unfolding. In addition, Raman spectroscopy indicates that the sulfhydryl group of each cysteine is a hydrogen bond donor in reduced thioredoxin (*41*). Hydrogen bonding by the sulfhydryl groups of the cysteine residues in reduced wild-type thioredoxin, which would be partially eliminated in the C32A and C35A point mutant proteins, may explain the slight thermodynamic destabilization of C32A and C35A relative to the reduced wild-type protein.

According to standard models, the *m* value reflects the change in the hydrophobic surface area exposed upon conversion of the native state to the denatured state (*42*). The low *m* value of IAALV relative to that of the wild type is consistent with a greater hydrophobic surface area exposed

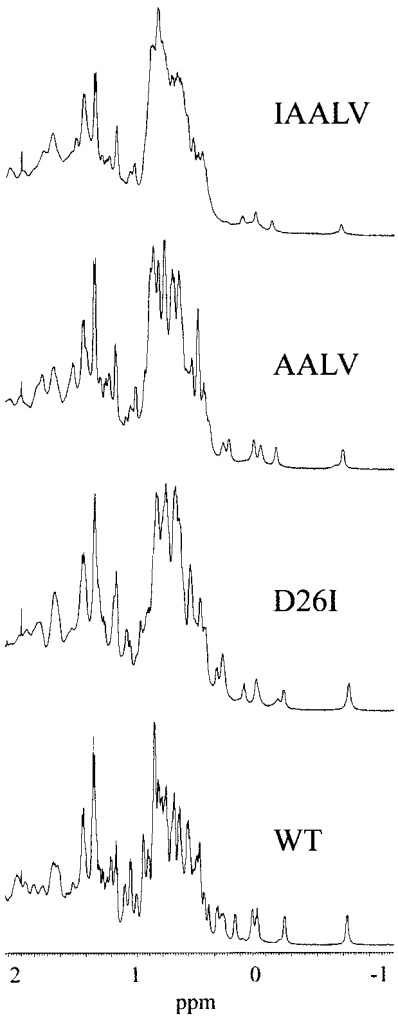

FIGURE 6: Proton NMR spectra of WT, D26I, AALV, and IAALV thioredoxin showing the upfield methyl region.

in the native state of IAALV than in wild-type thioredoxin. Fluctuation between multiple low-energy conformations in the native state may be responsible for some hydrophobic solvent exposure in IAALV. Decreased hydrophobic surface area exposed in the denatured state may also contribute to the low *m* value of IAALV relative to that of the wild type. Alternatively, the presence of folding intermediates, while not observed in comparing the extent of chemical denaturation determined in the circular dichroism and fluorescence experiments, may be responsible for the difference in *m* values between IAALV and wt.

The slight increase in the number of protected protons for D26I relative to wild-type thioredoxin indicates that the amide protons of D26I are less accessible to solvent. This observation is consistent with the increased thermodynamic stability of D26I relative to wild type. Both results suggest that D26I populates the unfolded state less than wild-type thioredoxin.

IAALV is thermodynamically stabilized relative to AALV; however, the level of this stabilization is greatly reduced compared to that of the D26I mutation in the wild-type background (1.1 and 3.1 kcal/mol, respectively). The extremely poor line shape and dispersion of IAALV relative to AALV indicates a substantial increase in conformational heterogeneity. Increased conformational heterogeneity could result in poor packing and is consistent with the reduced level of thermodynamic stabilization of the D26I mutation in the AALV background compared to the wild-type background. A small number of protons in IAALV are well protected from exchange with solvent, suggesting that in the family of folded structures putatively populated by IAALV these protons are continually inaccessible to solvent exchange. In contrast, AALV appears to be well structured in the folded state but samples the denatured state and fully exchanges all of its protons over the time course of the hydrogen exchange experiments. Adding the D26I mutation to AALV likely results in a family of low-energy structures in the folded state, all of which are stabilized relative to the denatured state.

Polar residues are prevalent at core positions in globular proteins. While some of these residues may be involved in active sites, the strong correlation with protein size suggests that most polar residues in the core are structurally important. McDonald and Thornton (*43*) found that the vast majority of buried polar atoms in proteins are satisfied by intramolecular hydrogen bonds. They conclude that to offset the energetic cost of losing H-bonds with solvent upon folding, the majority of buried polar groups observed in folded protein structures form intramolecular hydrogen bonds. Larger proteins are likely to require more polar core residues to satisfy the hydrogen bonding potential of buried polar groups on the backbone, which may explain part of the correlation between protein size and the number of polar residues at core positions.

Three slightly overlapping categories suffice to explain most core polar residues: active sites, thermodynamic stability, and structural specificity. Active sites use polar residues to perform chemistry and are often buried in clefts (*44*). Polar residues can increase thermodynamic stability when they form intramolecular hydrogen bonds to polar atoms that are solvent inaccessible (e.g., T66 and T77 in thioredoxin). The directional nature of polar interactions as well as their hydrophobic aversion allows core polar residues to determine a fold in a more specific manner than hydrophobic residues alone.

Previous studies have elucidated some of the factors that influence fold specificity. The relatively high level of conservation of core residues in sequence alignments clearly indicates the structural importance of core residues in terms of the hydrophobic effect and packing specificity (*45*). On the basis of this concept, a genetic library with the correct binary pattern to produce a 74-residue, four-helix bundle with a hydrophobic interior and hydrophilic exterior was shown to contain sequences that were helical and monomeric, and exhibited cooperative chemical denaturation (*46*). Consistent with these studies, we observe small proteins in our structural database survey with no polar residues at core positions. As the size of a protein increases, the probability of having a polar main chain atom that requires a core polar residue to satisfy its hydrogen bonding potential increases. Similarly, the number of folds that bury substantial hydrophobic surface area also increases with protein size. In larger proteins, polar residues at core positions likely aid in satisfying the hydrogen bond potential of main chain polar groups as well as energetically distinguishing a single well-folded structure from alternative structures.

ACKNOWLEDGMENT

We thank Scott Ross for guidance and assistance with NMR studies as well as useful discussions, and Arthur Street for compiling the data set analyzed in Figure 1.

REFERENCES

1. Chothia, C. (1976) *J. Mol. Biol. 105*, 1−14.
2. Miller, S., Janin, J., Lesk, A. M., and Chothia, C. (1987) *J. Mol. Biol. 196*, 641−656.
3. Dill, K. A. (1990) *Biochemistry 29*, 7133−7155.
4. Honig, B., and Yang, A. S. (1995) *Adv. Protein Chem. 46*, 27−58.
5. Malakauskas, S. M., and Mayo, S. L. (1998) *Nat. Struct. Biol. 5*, 470−475.
6. Eriksson, A. E., Baase, W. A., Zhang, X. J., Heinz, D. W., Blaber, M., Baldwin, E. P., and Matthews, B. W. (1992) *Science 255*, 178−183.
7. Dill, K. A., Bromberg, S., Yue, K., Fiebig, K. M., Yee, D. P., Thomas, P. D., and Chan, H. S. (1995) *Protein Sci. 4*, 561−602.
8. Dahiyat, B. I., and Mayo, S. L. (1997) *Science 278*, 82−87.
9. Nozaki, Y., and Tanford, C. (1971) *J. Biol. Chem. 246*, 2211−2217.
10. Lesser, G. J., and Rose, G. D. (1990) *Proteins 8*, 6−13.
11. Myers, J. K., and Pace, C. N. (1996) *Biophys. J. 71*, 2033−2039.
12. Blaber, M., Lindstrom, J. D., Gassner, N., Xu, J., Heinz, D. W., and Matthews, B. W. (1993) *Biochemistry 32*, 11363−11373.
13. Hendsch, Z. S., Jonsson, T., Sauer, R. T., and Tidor, B. (1996) *Biochemistry 35*, 7621−7625.
14. Hendsch, Z. S., and Tidor, B. (1994) *Protein Sci. 3*, 211−226.
15. Rose, G. D., and Wolfenden, R. (1993) *Annu. Rev. Biophys. Biomol. Struct. 22*, 381−415.
16. Byrne, M. P., Manuel, R. L., Lowe, L. G., and Stites, W. E. (1995) *Biochemistry 34*, 13949−13960.
17. Yamagata, Y., Kubota, M., Sumikawa, Y., Funahashi, J., Takano, K., Fujii, S., and Yutani, K. (1998) *Biochemistry 37*, 9355.
18. Takano, K., Yamagata, Y., Kubota, M., Funahashi, J., Fujii, S., and Yutani, K. (1999) *Biochemistry 38*, 6623−6629.
19. Shirley, B. A., Stanssens, P., Hahn, U., and Pace, C. N. (1992) *Biochemistry 31*, 725−732.
20. Pace, C. N., Shirley, B. A., McNutt, M., and Gajiwala, K. (1996) *FASEB J. 10*, 75−83.
21. O'Shea, E. K., Rutkowski, R., and Kim, P. S. (1992) *Cell 68*, 699−708.
22. O'Shea, E. K., Klemm, J. D., Kim, P. S., and Alber, T. (1991) *Science 254*, 539−544.
23. Harbury, P. B., Zhang, T., Kim, P. S., and Alber, T. (1993) *Science 262*, 1401−1407.
24. Gonzalez, L., Jr., Brown, R. A., Richardson, D., and Alber, T. (1996) *Nat. Struct. Biol. 3*, 1002−1009.
25. O'Shea, E. K., Lumb, K. J., and Kim, P. S. (1993) *Curr. Biol. 3*, 658−667.
26. Lumb, K. J., and Kim, P. S. (1995) *Biochemistry 34*, 8642−8648.
27. Munoz, V., and Serrano, L. (1994) *Proteins 20*, 301−311.
28. Katti, S. K., LeMaster, D. M., and Eklund, H. (1990) *J. Mol. Biol. 212*, 167−184.
29. Dahiyat, B. I., Sarisky, C. A., and Mayo, S. L. (1997) *J. Mol. Biol. 273*, 789−796.
30. Hemsley, A., Arnheim, N., Toney, M. D., Cortopassi, G., and Galas, D. J. (1989) *Nucleic Acids Res. 17*, 6545−6551.
31. Holmgren, A., and Reichard, P. (1967) *Eur. J. Biochem. 2*, 187−196.
32. Kelley, R. F., Shalongo, W., Jagannadham, M. V., and Stellwagen, E. (1987) *Biochemistry 26*, 1406−1411.
33. Santoro, M. M., and Bolen, D. W. (1988) *Biochemistry 27*, 8063−8068.
34. Privalov, G., Kavina, V., Freire, E., and Privalov, P. L. (1995) *Anal. Biochem. 232*, 79−85.
35. Kajander, T., Kahn, P. C., Passila, S. H., Cohen, D. C., Lehtio, L., Adolfsen, W., Warwicker, J., Schell, U., and Goldman, A. (2000) *Struct. Folding Des. 8*, 1203−1214.
36. Weichsel, A., Gasdaska, J. R., Powis, G., and Montfort, W. R. (1996) *Structure 4*, 735−751.
37. Nikkola, M., Gleason, F. K., Fuchs, J. A., and Eklund, H. (1993) *Biochemistry 32*, 5093−5098.
38. Andersen, J. F., Sanders, D. A., Gasdaska, J. R., Weichsel, A., Powis, G., and Montfort, W. R. (1997) *Biochemistry 36*, 13979−13988.
39. Langsetmo, K., Fuchs, J. A., and Woodward, C. (1991) *Biochemistry 30*, 7603−7609.
40. Ladbury, J. E., Kishore, N., Hellinga, H. W., Wynn, R., and Sturtevant, J. M. (1994) *Biochemistry 33*, 3688−3692.
41. Li, H., Hanson, C., Fuchs, J. A., Woodward, C., and Thomas, G. J., Jr. (1993) *Biochemistry 32*, 5800−5808.
42. Schellman, J. A. (1978) *Biopolymers 17*, 1305−1322.
43. McDonald, I. K., and Thornton, J. M. (1994) *J. Mol. Biol. 238*, 777−793.
44. Stryer, L. (1995) pp 191, W. H. Freeman and Company, New York.
45. Bowie, J. U., Reidhaar-Olson, J. F., Lim, W. A., and Sauer, R. T. (1990) *Science 247*, 1306−1310.
46. Kamtekar, S., Schiffer, J. M., Xiong, H., Babik, J. M., and Hecht, M. H. (1993) *Science 262*, 1680−1685.
47. Koradi, R., Billeter, M., and Wuthrich, K. (1996) *J. Mol. Graphics 14*, 51−55.
48. Zhang, Y. Z. (1995) in *Structural Biology and Molecular Biophysics*, pp 203, University of Pennsylvania, Philadelphia.
49. Bai, Y., Milne, J. S., Mayne, L., and Englander, S. W. (1993) *Proteins 17*, 75−86.

BI010427Y